Osteoarthritis and Cartilage 27 (2019) 823–832

Osteoarthritis and Cartilage

Changes in stiffness and biochemical composition of the pericellular matrix as a function of spatial chondrocyte organisation in osteoarthritic cartilage

M. Danalache †, R. Kleinert †, J. Schneider †, A.L. Erler † ‡, M. Schwitalle §, R. Riester †, F. Traub † ||, U.K. Hofmann † || *

† *Laboratory of Cell Biology, Department of Orthopaedic Surgery, University Hospital of Tübingen, Waldhörnlestraße 22, D-72072 Tübingen, Germany*
‡ *Medical Faculty of the University of Tübingen, D-72076 Tübingen, Germany*
§ *Winghofer Medicum, Röntgenstraße 38, D-72108 Rottenburg am Neckar, Germany*
|| *Department of Orthopaedic Surgery, University Hospital of Tübingen, Hoppe-Seyler-Strasse 3, D-72076 Tübingen, Germany*

ARTICLE INFO

Article history:
Received 17 June 2018
Accepted 20 January 2019

Keywords:
Osteoarthritis
Cellular organisation
Articular cartilage
Pericellular matrix
Atomic force microscopy
Stiffness

SUMMARY

Objective: During osteoarthritis (OA), chondrocytes seem to change their spatial arrangement from single to double strings, small and big clusters. Since the pericellular matrix (PCM) appears to degrade alongside this reorganisation, it has been suggested that spatial patterns act as an image-based biomarker for OA. The aim of this study was to establish the functional relevance of spatial organisation in articular cartilage.

Method: Cartilage samples were selected according to their predominant spatial cellular pattern. Young's modulus of their PCM was measured by atomic force microscopy (AFM) (~500 measurements/pattern). The distribution of two major PCM components (collagen type VI and perlecan) was analysed by immunohistochemistry (8 patients) and protein content quantified by enzyme-linked immunosorbent assay (ELISA) (58 patients).

Results: PCM stiffness significantly decreased with the development from single to double strings ($p = 0.030$), from double strings to small clusters ($p = 0.015$), and from small clusters to big clusters ($p < 0.001$). At the same time, the initially compact collagen type VI and perlecan staining progressively weakened and was less focalised. The earliest point with a significant reduction in protein content as shown by ELISA was the transition from single strings to small clusters for collagen type VI ($p = 0.016$) and from double strings to small clusters for perlecan ($p = 0.008$), with the lowest amounts for both proteins seen in big clusters.

Conclusions: This study demonstrates the functional relevance of spatial chondrocyte organisation as an image-based biomarker. At the transition from single to double strings PCM stiffness decreases, followed by protein degradation from double strings to small clusters.

Introduction

Articular cartilage is a specialised anisotropic connective tissue[1] composed of three layers: superficial, middle, and deep. Each of these layers is characterised by unique structural, functional, and biomechanical properties. Within the cartilage, chondrocytes form specific spatial patterns that are characteristic of each joint[2,3] and that appear to depend on joint-specific loading mechanisms[4]. The

Abbreviations: AFM, atomic force microscope; BC, big clusters; DS, double strings; DMEM, Dulbecco's modified Eagle's medium; ECM, extracellular matrix; ELISA, enzyme-linked immunosorbent assay; FDR, false discovery rate; OA, osteoarthritis; PBS, phosphate-buffered saline; PCM, pericellular matrix; SC, small clusters; SS, single strings.

* Address correspondence and reprint requests to: Laboratory of Cell Biology, Department of Orthopaedic Surgery, University Hospital of Tübingen, Waldhörnlestraße 22, D-72072 Tübingen, Germany.

E-mail addresses: danalachemarina@yahoo.com (M. Danalache), robinkleinert@web.de (R. Kleinert), 95janineschneider@gmail.com (J. Schneider), anna-lisa-erler@web.de (A.L. Erler), m.schwitalle@winghofer-medicum.de (M. Schwitalle), rosa.riester@med.uni-tuebingen.de (R. Riester), frank.traub@med.uni-tuebingen.de (F. Traub), ulf.hofmann@med.uni-tuebingen.de (U.K. Hofmann).

https://doi.org/10.1016/j.joca.2019.01.008
1063-4584/

predominant physiological cellular pattern found in the femoral condyle is that of single strings[5]. With osteoarthritis (OA) initiation and progression, spatial chondrocyte organisation changes: rearrangement can be observed from single strings to double strings[6], followed by small clusters, and finally big clusters[7]. In end-stage tissue degeneration, huge chondrocyte clusters are enclosed in densely packed tissue that is not well characterised[8,9]. This reorganisation of cellular spatial patterns has been suggested to act as an image-based biomarker for OA events occurring at a cellular level[4].

Characteristic for articular cartilage is the presence of a distinct and unique structure termed the pericellular matrix (PCM). The PCM has been primarily defined as the presence of collagen type VI[10,11]. It encompasses the chondrocytes, thus forming the structural, functional, and metabolic unit of articular cartilage termed the "chondron"[12]. Other key components of the PCM are the heparin-sulphate proteoglycan perlecan[13], aggrecan monomers[14] and aggregates[15], laminin[16], fibronectin[17], hyaluronan[18], biglycan[19], and collagen type IX[20]. The PCM acts as a mechano-sensitive cell matrix interface, protects the chondrocytes from apoptosis, and modulates biosynthetic response[21–23]. In contrast to the extracellular matrix (ECM), the PCM contains higher concentrations of proteoglycans[24], because, for example, the ECM proteoglycans biglycan and decorin bind near the N-terminal region of the collagen type VI triple helix[25]. The mesh-like capsule of the PCM defines its mechanical properties[26], which also determines the stiffness of the cartilage. Interestingly, the compressive mechanical properties also seem to depend on the position of the chondron within the cartilage[27].

OA onset is associated with collagen fibril denaturation[28,29] accompanied by a loss of small and large proteoglycans[30]. Local changes in perlecan expression and content have also been reported during OA development[31]. The loss of these molecules is correlated with the presence and elevated activity of various matrix metalloproteinases[32,33]. As a result, despite the fact that the expression of collagen is upregulated[34], the net amount of, for example, collagen type II in the ECM decreases[35,36]. Similar changes during OA have also been described specifically for collagen type VI: in the lower middle and upper deep zones of the articular cartilage, its expression and presence seems to increase; in the upper middle zone, it appears to be lost; and in the superficial zone, it shows heterogeneous expression[7,37].

Our aim in the present study was to evaluate the biomechanical degenerative changes of the PCM from human articular cartilage explants through determination of Young's moduli (stiffness) by using the spatial organisation of chondrocytes as an image-based biomarker. To evaluate the biomechanical properties of articular cartilage, we used atomic force microscopy (AFM), which is a powerful technique that allows direct quantification of the biomechanical tissue properties *in situ* at a microscale with minimal risk of interfering with its natural physiological state[38]. We also analysed the associated changes in PCM composition by examining two of its main components: collagen type VI and perlecan. We hypothesised (I) that the more pathological the spatial chondrocyte arrangement, the lower the stiffness of the cellular microenvironment and (II) that the presence of collagen type VI and perlecan would decrease with increasing tissue destruction.

Materials and methods

Cartilage samples

Tissue was obtained from patients undergoing total knee arthroplasty in the Department of Orthopaedic Surgery of the University Hospital of Tuebingen, Germany, and the Winghofer-clinic, Rottenburg a.N., Germany, for end-stage OA of the knee. Full departmental, institutional, and local ethical committee approval were obtained before commencement of the study (project number 674/2016BO2). Written informed consent was received from all patients before participation.

Tissue sample preparation for AFM testing

After surgery resection, the tissue was temporarily stored in serum-free Dulbecco's modified Eagle's medium (DMEM; Gibco, Life Technologies, Darmstadt, Germany) with 2 % (v/v) penicillin-streptomycin and 1.2 % (v/v) amphotericin B. Full-thickness articular cartilage samples were then collected and embedded in water-soluble embedding medium (Tissue-Tek O.C.T. Compound, Sakura Finetek, Alphen aan den Rijn, Netherlands). Sectioning of the topmost layer of articular cartilage (representing the first 300 μm) was performed with a Leica cryotome type CM3050S (Leica Biosystems, Wetzlar, Germany) with 35 μm thickness ($n = 4$ cuts per patient). Cartilage slices were rinsed with phosphate-buffered saline (PBS) to remove the water-soluble embedding medium, glued (biocompatible sample glue, JPK Instruments AG, Berlin, Germany) onto tissue culture dishes (TPP Techno Plastic Products AG, Trasadingen, Switzerland), and covered with Leibovitz's L-15 medium w/o L-glutamine (Merck KGaA, Darmstadt, Germany) until AFM measurements. Processing of the cartilage samples and the AFM measurements was done immediately after tissue resection to reduce artefacts from swelling of the tissue.

Biomechanical characterisation of the PCM via AFM

Elastic moduli of the PCM were assessed by using an AFM system (CellHesion 200, JPK Instruments, Berlin, Germany) integrated into an inverted phase contrast microscope (AxioObserver D1, Carl Zeiss Microscopy, Jena, Germany), which allowed simultaneous visualisation of the cartilage samples. This allowed us to measure specific cellular spatial patterns. Calibration of the cantilever was done on the retracted curve, and the spring constant was determined by using the thermal noise method incorporated into the device software (JPK Instruments, Berlin, Germany). Measurements were performed in force spectroscopy mode by recording single force–distance curves at the position of interest without laterally scanning the sample. For microscale indentation, a polymeric microsphere (25 μm in diameter, Polysciences, Inc., Warrington, PA, USA) was attached to an AFM cantilever (tip C, $k = 7.4$ N/m, All-In-One-Al–Tl, Budget Sensors, Sofia, Bulgaria). Indentation curves were sampled at 2 kHz, with a force trigger of ~300 nN and a velocity of 5 μm/s. To evaluate elastic properties of the PCM as a function of the cellular spatial organisation, we applied indentations over the chosen region of interest identified by microscopic examination (9 measurement repetitions/measurement site; two distinct cellular patterns/histologic cut) (Fig. 1). In case a pattern was not present on a histologic cut, this measurement was left out. Young's modulus was calculated from the force–distance curves by using the Hertz-fit model of the data processing software (JPK Instruments, Berlin, Germany). Young's modulus is the ratio of uniaxial force per unit surface in pascal divided by the adimensional proportional deformation of the examined tissue.

PCM immunostaining

Following AFM measurements, cartilage samples were fixed with 4 % (w/v) paraformaldehyde in PBS for 30 min at room temperature, and then processed and labelled for collagen type VI and perlecan. Enzymatic pretreatment of samples was done as

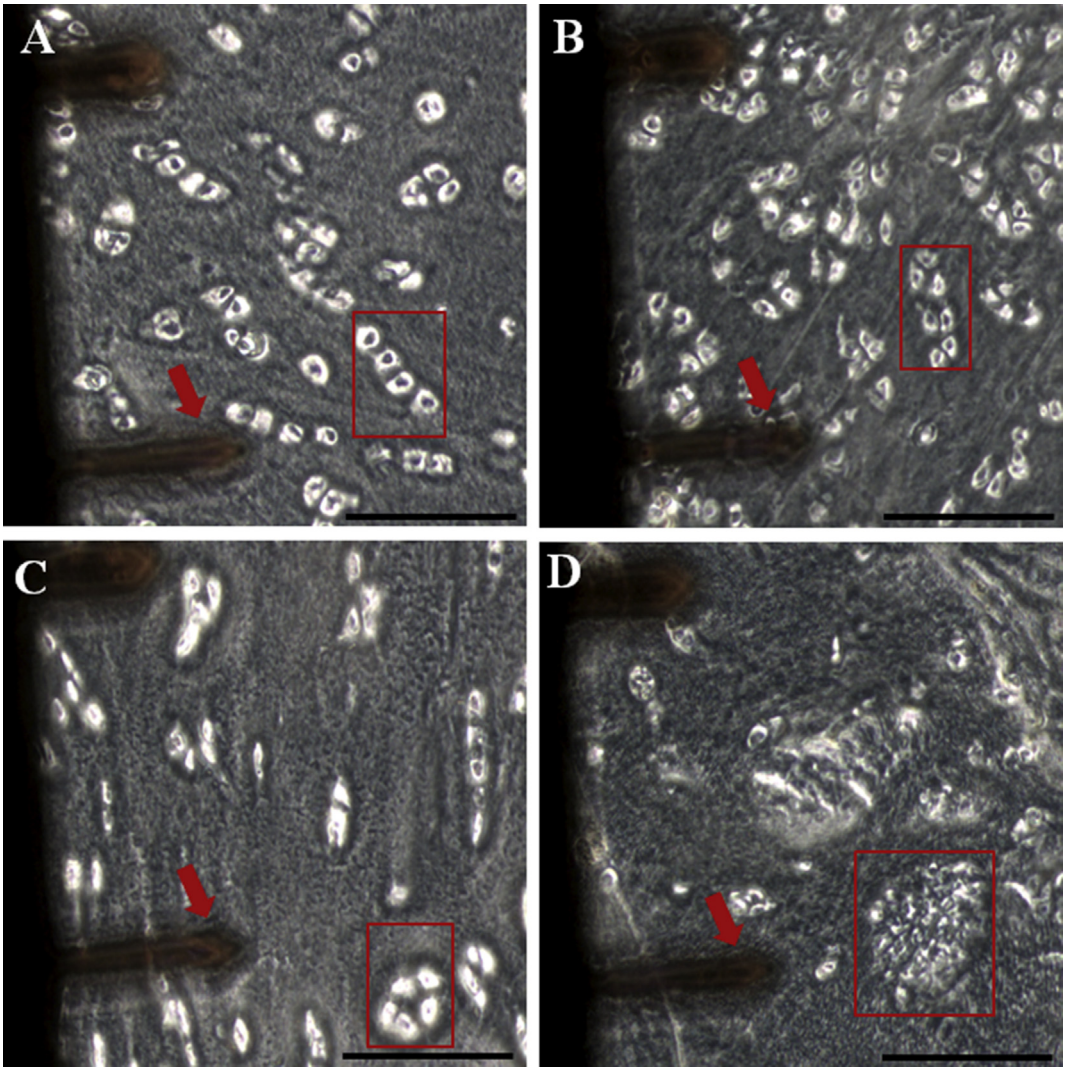

Fig. 1. Light microscopy pictures indicating regions of interest. atomic force microscopy (AFM) pictures showing the distinct cellular spatial patterns of strings (**A**), double strings (**B**), small clusters (**C**), and big clusters (**D**) (red box). Red arrow showing the cantilever that was used. Scale bar (black) represents 150 μm.

previously described[39,40] with some modifications. Briefly, histological sections were pretreated with 0.1 % (w/v) hyaluronidase (Sigma–Aldrich, Taufkirchen, Germany) for perlecan staining and 0.2 % (w/v) collagenase type XI (Sigma–Aldrich, Taufkirchen, Germany) for collagen type VI staining in PBS at 37°C for 1 h, followed by three washing steps with PBS. Sections were incubated with a mix of 5 % (w/v) bovine serum albumin and 0.3 % (v/v) Triton X-100 in PBS as a blocking agent for 30 min, followed by incubation with collagen type VI (rabbit anti-collagen VI, ab-182744, Abcam, Cambridge, UK) and perlecan (mouse anti-perlecan, sc-377219, Santa Cruz Biotechnology Inc., Dallas, TX, USA) primary monoclonal antibodies at a dilution of 1:100 in 2.5 % (w/v) bovine serum albumin-PBS overnight at 4°C in a humidity chamber. Afterwards, sections were incubated with secondary antibodies (Alexa Fluor 555 goat anti-rabbit IgG, a-21429, Thermo Scientific, Waltham, MA, USA, and Alexa Fluor 594 goat anti-mouse IgG, ab-150116, Abcam, Cambridge, UK) for 2 h with a dilution of 1:100 at room temperature in the dark. Nuclear staining was performed with 1 % (v/v) DAPI in PBS for 5 min prior to imaging. Fluorescence-stained tissue sections were visualised with a Carl Zeiss Observer Z1 fluorescence microscope (Carl Zeiss Microscopy, Jena, Germany).

Tissue preparation for biochemical quantification of the PCM

Thin pieces of articular cartilage were cut with a scalpel blade no. 21 from the surface of the femoral condyle. A self-made cutting device was used to generate 300 μm discs of tissue representing the top-most layer of articular cartilage. Fresh-cut pieces of articular cartilage from each patient were stained with 4μM Calcein AM fluorescence dye (Cayman Chemical, Ann Arbor, Michigan, USA) in serum-free DMEM (Gibco, Life Technologies, Darmstadt, Germany) with 2 % (v/v) penicillin-streptomycin and 1.2 % (v/v) amphotericin B for 30 min at 37°C. Calcein-stained samples were visually classified and sorted according to their predominant cellular spatial patterns[41] by using a fluorescence microscope (Leica DM IMBRE, Germany). Discs were then assigned to each of the four individual cellular spatial pattern groups. The discs were then snap-frozen in liquid nitrogen and stored at −80°C until further analysis.

Assessment of PCM components by enzyme-linked immunosorbent assay (ELISA)

Frozen cartilage explants from each group were crushed with a pestle and mortar under liquid nitrogen and placed on ice for

15 min in homogenisation buffer (25 mM Tris–HCl pH 7.5, 100 mM NaCl, 1 % (v/v) IGEPAL CA-630) supplemented with proteinase inhibitors. A soluble fraction was obtained by centrifugation at 15,000*g* for 15 min at 4°C. For normalisation of the amount of tissue, aliquots were first analysed for total protein concentration by Bradford protein assay (Bio-Rad Laboratories, Richmond, CA, USA). A total of 15 μg of protein for each individual cellular pattern was subjected to sandwich ELISA for collagen type VI (MyBiosource Inc., San Diego, CA, USA) and 10 μg of protein for perlecan (BIOZOL Diagnostica Vertrieb GmbH, Eching, Germany) following the manufacturer's protocol. Absorbance was recorded at 450 nm by using an EL 800 reader (BioTek Instruments GmbH, Bad Friedrichshall, Germany). Protein content was calculated from the absorbance according to the prior established protein specific standard absorption curve. Three independent measurements of the ELISA assays were performed for each spatial pattern.

Statistical analysis

Normality of the data was assessed by histograms. For further analyses, the median of the nine AFM measurements per measurement site was used. Extreme values were screened and filtered by the 2-standard deviation (SD) method. Depending on normality, values are presented as median (minimum–maximum) and graphically displayed as boxplots, or as mean (SD) and graphically displayed as bar diagrams. Even though our AFM results were not normally distributed, the mean, SD, and standard error of the mean of the AFM data are additionally displayed (Table II) to allow a direct comparison of our results with those reported in the literature.

To further analyse the results, the same approach and assumptions were employed as described previously by Wilusz *et al.*[42]: Briefly, each median of the nine AFM measurements per measurement site was treated as an independent value within each group of cellular spatial pattern. This assumption could be made as cartilage biomechanical properties display "greater variations spatially than among individuals"[42]. The biomechanical properties of the articular cartilage are prone to significant spatial variations across the joint[43], also varying with depth from the articular surface[44] and they are influenced by loading changes occurring during joint motion[45]. Since measured regions were chosen over the entire length of each sample and were not adjacent to one another, it is extremely unlikely that the measured regions within the same joint would have experienced the same biomechanical environment *in situ* or been influenced by each other.

Comparison between experimental results was therefore performed with the Kruskal–Wallis test by using the Mann-Whitney *U* test for *post hoc* analysis, or by one-way analysis of variance and *t*-test for independent samples as a *post hoc* test, as appropriate. Alpha adjustment on the basis of a significance level of 0.05 was performed for each calculation by using the Benjamini-Hochberg procedure. Statistical analysis was performed with SPSS Statistics 22 (IBM Corp., Armonk, NY, USA).

Table I
Comparison of elasticity measurements (Young's modulus) as a function of cellular spatial organisation

Comparison	*P*-value	FDR-adjusted alpha values
All Groups	<0.001*	<0.001
SS–DS	0.030°	0.030
SS–SC	<0.001°	<0.001
SS–BC	<0.001°	<0.001
DS–SC	0.013°	0.015
DS–BC	<0.001°	<0.001
SC–BC	<0.001°	<0.001

*Kruskal–Wallis test, °Mann-Whitney *U* test. Abbreviations: SS – single strings; DS – double strings; SC – small clusters; BC – big clusters; FDR – false discovery rate.

Table II
Stiffness measurements by atomic force microscopy (AFM)

Descriptive statistics	Cellular organisational pattern			
	SS	DS	SC	BC
Median	37.611	25.330	13.714	5.643
Minimum	5.447	2.581	0.500	0.332
Maximum	174.315	122.213	58.066	24.487
Mean	49.479	33.828	18.983	7.615
Standard deviation	40.376	29.159	14.161	5.849
Standard error	5.395	4.043	1.909	0.788

Values displayed in kPa. Abbreviations: SS – single strings; DS – double strings; SC – small clusters; BC – big clusters.

Results

Articular cartilage samples from eight patients were subjected to elasticity measurements of the pericellular region via AFM. Thus, a total of 2070 measurements were done (single strings: 513, double strings: 504, small clusters: 531, big clusters: 522). After exclusion of extreme values, the median for 56 single strings, 52 double strings, 55 small clusters, and 55 big clusters were included in the final analysis. The measured PCM elastic moduli results are shown in Fig. 2 and Table I. Stiffness of the patterns significantly decreased along the entire scale of patterns from single strings to double strings ($p = 0.030$), from double strings to small clusters ($p = 0.015$), and from small clusters to big clusters ($p < 0.001$). Absolute values were thereby reduced by 84 % with a median of 38 kPa for single strings to a median of 6 kPa for big clusters.

In the immunofluorescence analysis, healthy tissue areas represented by single strings exhibited a PCM composed of densely compact, intact, and well-defined collagen type VI [Fig. 3(A)] and perlecan [Fig. 3(E)]. With initiation and progression of tissue degeneration represented by the cellular pattern shift from single strings (Fig. 3(A/E)) to double strings (Fig. 3(B/F)) to small clusters (Fig. 3(C/G)) and eventually to big clusters (Fig. 3(D/H)), a change in staining localisation and integrity of collagen type VI was observed and, to a lesser extent, of perlecan: the PCM contour around the chondrocytes softened, especially for collagen type VI immunolabelling. Moreover, PCM staining of collagen type VI no longer exhibited a precise localisation restricted to the pericellular region of the chondrocytes; rather, it was scattered between the cells. By comparison, in advanced tissue degeneration represented by chondrocyte clustering (small and big clusters), perlecan was still present and localised in the PCM.

Tissue samples from 58 patients ($n = 25$ for collagen type VI assays and $n = 33$ for perlecan assays) were included in the ELISA analysis. Since not all patients presented all spatial patterns, 46–52 cartilage discs per pattern for collagen type VI and perlecan were used. Complementary to immunolabelling, quantitative ELISA analyses showed that the more pathological the cellular pattern, the more collagen type VI (Fig. 4(A)) and perlecan (Fig. 4(B)) decreased. The earliest point in the sequence of events where a significant reduction could be observed was the transition from single strings to small clusters for collagen type VI ($p = 0.016$) and for perlecan ($p = 0.008$) (Table III and Table IV). For both collagen type VI and perlecan, the lowest amounts were measured in big clusters.

Discussion

The aim of this study was to evaluate whether stiffness of the PCM decreases as a function of OA initiation and progression by using the spatial arrangement of chondrocytes as an image-based

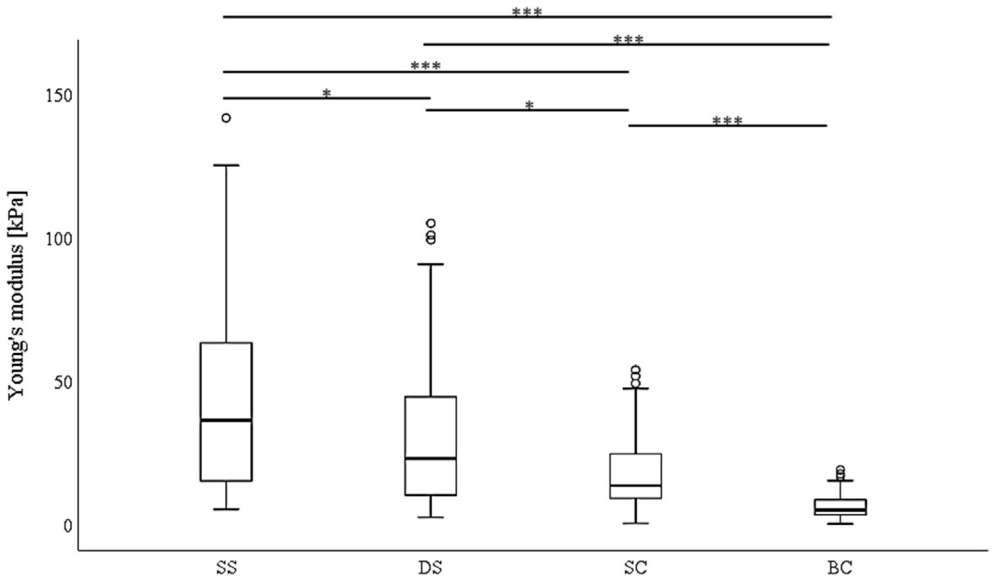

Fig. 2. Comparison of quantified Young's modulus of the pericellular matrix (PCM) as a function of cellular organisation. Boxplots of the stiffness measured by AFM of the different chondrocyte patterns. A continuous reduction of stiffness in the PCM during the rearrangement from the SS to the BC pattern can be observed. $^{*}p < 0.05$; $^{***}p < 0.001$ (for exact *P*-values, see Table I). Abbreviations: SS – single strings; DS – double strings; SC – small clusters; BC – big clusters.

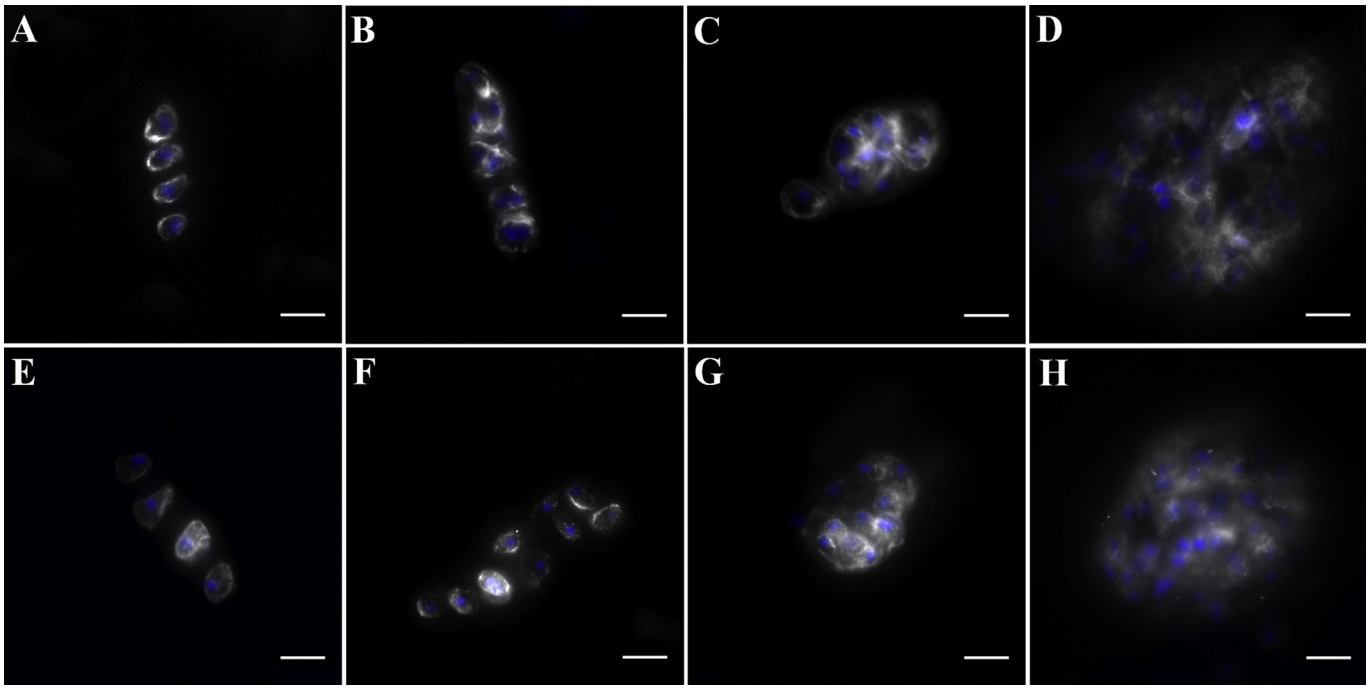

Fig. 3. PCM immunolabelling for collagen type VI and perlecan for the different cellular spatial patterns. Immunolabelled PCM with Alexa Fluor 555 anti-collagen type VI antibody (**A**–**D**) and Alexa Fluor 594 anti-perlecan antibody (**A**/**E** – single strings, **B**/**F** – double strings, **C**/**G** – small clusters, **D**/**H** – big clusters). While a decrease in collagen type VI from single strings to big clusters can be observed (**A**–**D**), the intensity of the decrease for perlecan is much less pronounced (**E**–**H**). 20-fold magnification, scale bar represents 20 μm.

biomarker. We found that the more pathological the spatial arrangement of the chondrocytes, the lower the stiffness of the single chondron (hypothesis I). This translates into a total difference in the mean of Young's modulus of 30 kPa (~60 %) between single strings and small clusters, and of 41 kPa between single strings and big clusters (~80 %). The results of our stiffness measurements of supposedly healthy cartilage (i.e., single strings) are comparable to data from previous publications for native healthy articular cartilage[46,47]. The same applies to small clusters when we compared them with the values obtained by Wilusz *et al.* (2013), where the PCM from early OA cartilage was measured[42]. A comparable 30–40 % decrease in the PCM moduli was also reported when we measured chondrons extracted by micropipette aspiration of OA cartilage and of macroscopically intact tissue[8,48]. Interestingly, the earliest statistically significant decrease observed in our AFM data was at the first possible time point: the transition from single to double strings ($p = 0.030$, Table I). Since double strings are a feature most commonly observed in macroscopically intact cartilage[6], this underlines the biomechanical relevance of spatial organisation as a functional biomarker.

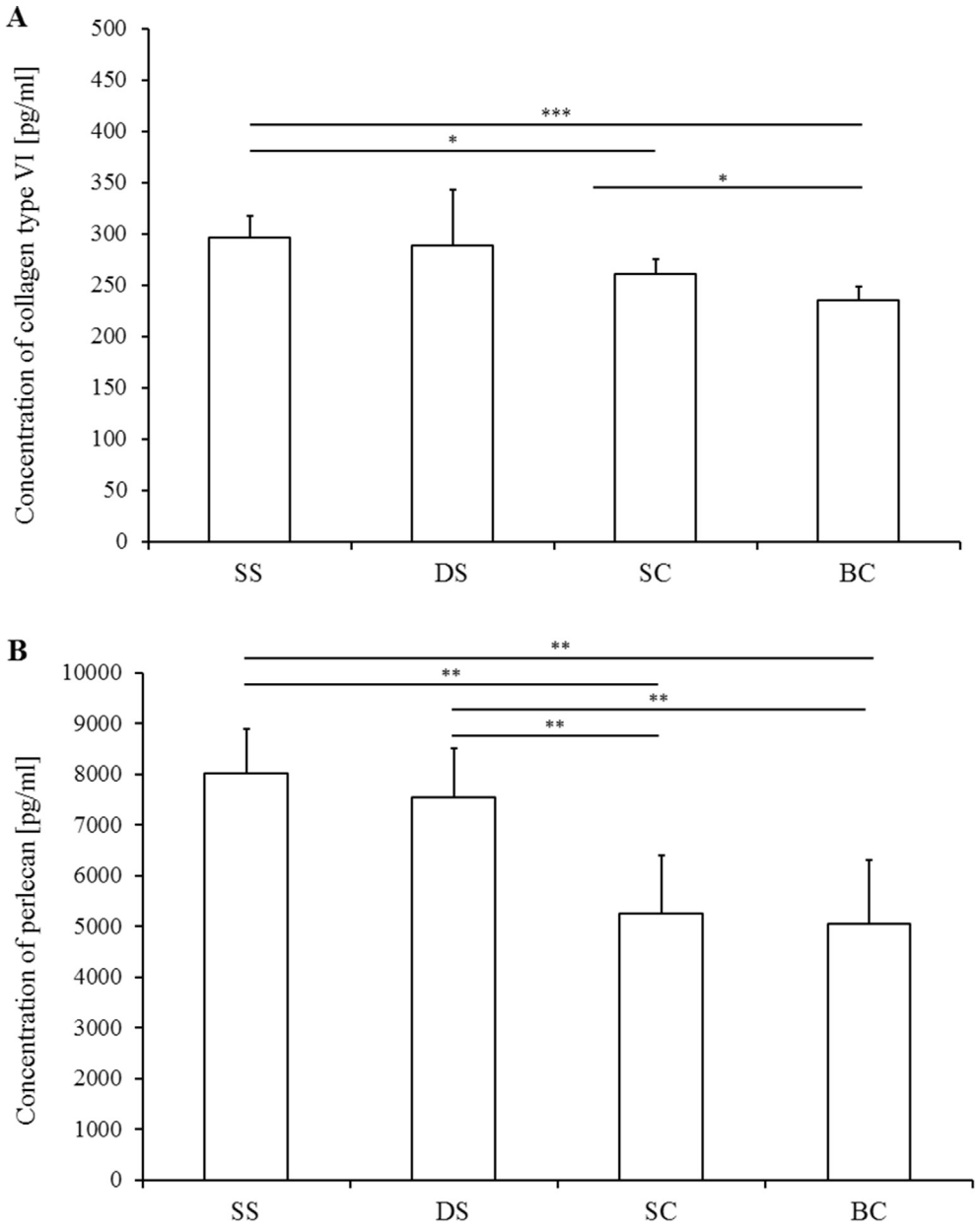

Fig. 4. Biochemical analysis of the PCM by quantification of collagen type VI and perlecan as a function of cellular pattern organisation. ELISAs performed with homogenised cartilage to quantify changes in content of collagen type VI (**A**) and perlecan (**B**) according to the predominant spatial cellular pattern. From single strings to big clusters, a decrease in collagen type VI and a significantly lower amount of perlecan can be observed in small clusters and big clusters compared with that in single strings and double strings. $^{*}p < 0.05$; $^{**}p < 0.01$; $^{***}p < 0.001$. Abbreviations: SS – single strings; DS – double strings; SC – small clusters; BC – big clusters.

Table III
Comparison of ELISA assays for collagen type VI as a function of cellular spatial organisation

Comparison	*P*-value	FDR-adjusted alpha values
All Groups	0.010*	0.017
SS–DS	0.739°	0.739
SS–SC	0.007°	0.016
SS–BC	<0.001°	<0.001
DS–SC	0.267°	0.311
DS–BC	0.042°	0.058
SC–BC	0.004°	0.014

*ANOVA, °*t*-test for independent samples. Abbreviations: SS – single strings; DS – double strings; SC – small clusters; BC – big clusters; FDR – false discovery rate.

Table IV
Comparison of ELISA assays for perlecan as a function of cellular spatial organisation

Comparison	*P*-value	FDR-adjusted alpha values
All Groups	0.002*	0.004
SS–DS	0.393°	0.458
SS–SC	0.001°	0.003
SS–BC	<0.001°	0.003
DS–SC	0.006°	0.008
DS–BC	0.003°	0.005
SC–BC	0.790°	0.790

*ANOVA, °*t*-test for independent samples. Abbreviations: SS – single strings; DS – double strings; SC – small clusters; BC – big clusters; FDR – false discovery rate.

We also analysed the changes in PCM composition accompanying spatial rearrangement by examining two of its main components: collagen type VI and perlecan. As previously described, collagen type VI[10,49] and perlecan[50] were present at high levels in single strings representing healthy cartilage. As hypothesised (hypothesis II), ELISA analyses showed that the protein content decreased in conjunction with the spatial physiopathological model. In this case, the earliest point in the sequence of events with a significant protein content reduction was at the transition from single strings to small clusters for collagen type VI ($p = 0.016$) and from double strings to small clusters for perlecan ($p = 0.008$) (Tables III and IV). In the immunohistological analyses, the PCM contour around the chondrocytes also softened with increasingly pathological spatial organisation. In particular, in small and large clusters, collagen type VI and perlecan staining was no longer clearly restricted to the pericellular region, but also showed a diffuse blur between adjacent cells. The reasons for this observation remain, so far, speculative. The observed nonhomogeneous distribution of collagen type VI is most likely the consequence of nonhomogeneous degradation of collagen type VI occurring in OA[37]. The loss of perlecan from the PCM could be due to an inflammatory change in β1 integrin, as it is suggested to mediate interactions between the cell surface and perlecan[51–53].

Several publications have linked the PCM to biomechanical functions in tensional and load-bearing connective tissue[27,46,47,54–56], indicating that the PCM acts as transducer of mechanical and physicochemical signals[21,57] and that it is susceptible to OA triggered degenerative changes[58]. It has also been reported that collagen type VI[59,60] is reduced and perlecan is altered in OA[31]. We are the first, however, to describe these changes as a function of cellular spatial rearrangement. The decrease in PCM stiffness that is observed simultaneously with the reduction in collagen type VI and perlecan suggests that these two phenomena are linked to each other. This idea is supported by the observation that knockdown collagen type VI mice also exhibit lower PCM elastic moduli, and, at the same time, show increased chondrocyte swelling[57]. With respect to the role of perlecan, Xu *et al.* (2016) showed in a murine model of Schwartz-Jampel syndrome that perlecan knockdown alters matrix organisation and causes a reduction in stiffness[61]. In 2012, Wilusz *et al.* reported that isolated enzymatic depletion of perlecan increases PCM elastic moduli, pointing out the possible involvement of perlecan in biomechanical properties[62]. To explain this unexpected finding, they used the analogy of a spring system in series with a stiffer and a softer spring, where "the effective spring constant of the system is lower than the spring constant of either component[62]". In our study, a decrease in perlecan led to a reduction in stiffness. Yet at the same time, we also observed a decrease in collagen type VI, which – continuing with Wilusz's analogy – would also lower the second spring stiffness. From the present data, the question remains open to discussion whether a spring system in series would in fact illustrate the observed phenomenon, or whether instead the perlecan and collagen type VI are somehow functionally intertwined, the isolated depletion of perlecan leading to an increase in stiffness of the collagen type VI fibres. It will also be interesting to investigate how the PCM is connected microbiomechanically with the ECM and if disruption of the PCM correlates also with changes in ECM elasticity during degeneration.

Of note, the AFM data show significant reductions in stiffness between all of the spatial chondrocyte patterns. The decrease in protein quantity is first measured at the change from double strings to small clusters. While the elasticity of the PCM is thus already clearly affected from the earliest rearrangement on, this is not immediately translated into a reduction in protein content. One simple explanatory approach to this phenomenon could be that at the transition from single to double strings, the number of cells within a defined cartilage area increases. While the total protein content for key PCM components remains at a similar level, this means that the amount of protein available per PCM per cell would be reduced, leading to an early reduction in PCM mechanical moduli. Alternatively, at the transition from single to double strings, collagen type VI and perlecan might be fragmented without being degraded. Söder *et al.* (2002) suggested that two types of collagen type VI destruction occur in osteoarthritic cartilage: induced molecular degradation resulting in the diffusion of collagen type VI fragments into the adjacent interterritorial matrix, and transformation of collagen type VI filaments to banded structures that no longer provide the flexible mechanical interface to the ECM-collagen type II[63].

Since spatial chondrocyte organisation indeed has functional relevance, the impact of this image-based biomarker is strongly enhanced. Our data affirm that first degenerative changes are already measurable functionally at the transition from single to double strings, where macroscopically the cartilage still appears intact. This implies that such a biomarker could be used for diagnosis of early stages of OA. If researchers use regenerative therapies to pursue the goal of recreating physiological cartilage architecture, this model can also serve as a landmark parameter, with single strings being the target organisational form in the cellular reorganisation process.

Study limitations

Values from AFM measurements show a relevant individual range between patterns as well as in repeated measurements. This phenomenon can be counteracted by choosing a large sample size as we did in our study. One possible explanation for the variation in values for the same patterns may be the regional variation in biomechanical properties of the PCM[47]. Experimental parameters used for mechanical testing, such as indentation velocity and depth, indenter shape and size, and accurate representation of tip geometry in model fitting[64] may impact absolute values of the measured mechanical properties[65,66]. They should not, however, affect the results within one study and their relation to each other.

Conclusion

This study demonstrates the functional relevance of using spatial chondrocyte organisation as an image-based biomarker. At the transition from single to double strings, PCM stiffness is beginning to decrease, where macroscopically the cartilage still appears intact. This is followed by a reduction in collagen type VI and perlecan content, suggesting that the degeneration of these components and functional disruption of the PCM are closely intertwined events in OA physiopathology.

Authors' contribution

MD designed the study, performed the experiments, did the statistical analyses, and wrote the manuscript; RK helped interpret the data and to write the manuscript; JS performed the experiments and helped with the statistical analyses; ALE helped with the immunohistochemistry and the statistical analyses; MS provided the cartilage samples, helped interpret the data, and critically revised the manuscript; RR helped perform the experiments; FT helped design the study and write the manuscript; and UKH designed and supervised the study, helped with the statistical analyses, and wrote the manuscript. All authors read and approved the final manuscript.

Conflict of interest

All authors declare that they have no conflict of interest.

Role of the funding source

No funding was received for the study.

Acknowledgements

We thank the orthopaedic surgeons from the Department of Orthopaedic Surgery of the University Hospital of Tuebingen and from Winghofer-Clinic/Rottenburg for providing the tissue samples. We thank Barbara Every, ELS, of BioMedical Editor, for English language editing.

References

1. Heinegard D, Oldberg A. Structure and biology of cartilage and bone matrix noncollagenous macromolecules. FASEB J 1989;3:2042–51.
2. Rolauffs B, Williams JM, Grodzinsky AJ, Kuettner KE, Cole AA. Distinct horizontal patterns in the spatial organization of superficial zone chondrocytes of human joints. J Struct Biol 2008;162:335–44.
3. Schumacher BL, Su JL, Lindley KM, Kuettner KE, Cole AA. Horizontally oriented clusters of multiple chondrons in the superficial zone of ankle, but not knee articular cartilage. Anat Rec 2002;266:241–8.
4. Rolauffs B, Rothdiener M, Bahrs C, Badke A, Weise K, Kuettner KE, *et al*. Onset of preclinical osteoarthritis: the angular spatial organization permits early diagnosis. Arthritis Rheum 2011;63:1637–47.
5. Aicher WK, Rolauffs B. The spatial organisation of joint surface chondrocytes: review of its potential roles in tissue functioning, disease and early, preclinical diagnosis of osteoarthritis. Ann Rheum Dis 2014;73:645–53.
6. Rolauffs B, Williams JM, Aurich M, Grodzinsky AJ, Kuettner KE, Cole AA. Proliferative remodeling of the spatial organization of human superficial chondrocytes distant from focal early osteoarthritis. Arthritis Rheum 2010;62:489–98.
7. Felka T, Rothdiener M, Bast S, Uynuk-Ool T, Zouhair S, Ochs BG, *et al*. Loss of spatial organization and destruction of the pericellular matrix in early osteoarthritis in vivo and in a novel in vitro methodology. Osteoarthritis Cartilage 2016;24:1200–9.
8. Alexopoulos LG, Haider MA, Vail TP, Guilak F. Alterations in the mechanical properties of the human chondrocyte pericellular matrix with osteoarthritis. J Biomech Eng 2003;125:323–33.
9. Hellio Le Graverand MP, Sciore P, Eggerer J, Rattner JP, Vignon E, Barclay L, *et al*. Formation and phenotype of cell clusters in osteoarthritic meniscus. Arthritis Rheum 2001;44:1808–18.
10. Poole CA, Ayad S, Gilbert RT. Chondrons from articular cartilage. V. Immunohistochemical evaluation of type VI collagen organisation in isolated chondrons by light, confocal and electron microscopy. J Cell Sci 1992;103(Pt 4):1101–10.
11. Youn I, Choi JB, Cao L, Setton LA, Guilak F. Zonal variations in the three-dimensional morphology of the chondron measured in situ using confocal microscopy. Osteoarthritis Cartilage 2006;14:889–97.
12. Poole CA. Articular cartilage chondrons: form, function and failure. J Anat 1997;191(Pt 1):1–13.
13. Melrose J, Hayes AJ, Whitelock JM, Little CB. Perlecan, the "jack of all trades" proteoglycan of cartilaginous weight-bearing connective tissues. Bioessays 2008;30:457–69.
14. Knudson W, Ishizuka S, Terabe K, Askew EB, Knudson CB. The pericellular hyaluronan of articular chondrocytes. Matrix Biol 2018, https://doi.org/10.1016/j.matbio.2018.02.005. in press.
15. Poole AR, Pidoux I, Reiner A, Rosenberg L. An immunoelectron microscope study of the organization of proteoglycan monomer, link protein, and collagen in the matrix of articular cartilage. J Cell Biol 1982;93:921–37.
16. Durr J, Lammi P, Goodman SL, Aigner T, von der Mark K. Identification and immunolocalization of laminin in cartilage. Exp Cell Res 1996;222:225–33.
17. Chang J, Nakajima H, Poole CA. Structural colocalisation of type VI collagen and fibronectin in agarose cultured chondrocytes and isolated chondrons extracted from adult canine tibial cartilage. J Anat 1997;190(Pt 4):523–32.
18. Poole CA, Glant TT, Schofield JR. Chondrons from articular cartilage. (IV). Immunolocalization of proteoglycan epitopes in isolated canine tibial chondrons. J Histochem Cytochem 1991;39:1175–87.
19. Kavanagh E, Ashhurst DE. Development and aging of the articular cartilage of the rabbit knee joint: distribution of biglycan, decorin, and matrilin-1. J Histochem Cytochem 1999;47:1603–16.
20. Poole CA, Gilbert RT, Herbage D, Hartmann DJ. Immunolocalization of type IX collagen in normal and spontaneously osteoarthritic canine tibial cartilage and isolated chondrons. Osteoarthritis Cartilage 1997;5:191–204.
21. Guilak F, Alexopoulos LG, Upton ML, Youn I, Choi JB, Cao L, *et al*. The pericellular matrix as a transducer of biomechanical and biochemical signals in articular cartilage. Ann N Y Acad Sci 2006;1068:498–512.
22. Peters HC, Otto TJ, Enders JT, Jin W, Moed BR, Zhang Z. The protective role of the pericellular matrix in chondrocyte apoptosis. Tissue Eng 2011;17:2017–24.
23. Larson CM, Kelley SS, Blackwood AD, Banes AJ, Lee GM. Retention of the native chondrocyte pericellular matrix results in significantly improved matrix production. Matrix Biol 2002;21:349–59.
24. Poole CA, Flint MH, Beaumont BW. Morphological and functional interrelationships of articular cartilage matrices. J Anat 1984;138(Pt 1):113–38.
25. Wiberg C, Hedbom E, Khairullina A, Lamande SR, Oldberg A, Timpl R, *et al*. Biglycan and decorin bind close to the n-terminal region of the collagen VI triple helix. J Biol Chem 2001;276:18947–52.
26. Poole CA, Flint MH, Beaumont BW. Chondrons in cartilage: ultrastructural analysis of the pericellular microenvironment in adult human articular cartilages. J Orthop Res 1987;5:509–22.
27. Choi JB, Youn I, Cao L, Leddy HA, Gilchrist CL, Setton LA, *et al*. Zonal changes in the three-dimensional morphology of the chondron under compression: the relationship among cellular, pericellular, and extracellular deformation in articular cartilage. J Biomech 2007;40:2596–603.
28. Hollander AP, Pidoux I, Reiner A, Rorabeck C, Bourne R, Poole AR. Damage to type II collagen in aging and osteoarthritis starts at the articular surface, originates around chondrocytes, and extends into the cartilage with progressive degeneration. J Clin Invest 1995;96:2859–69.
29. Poole AR. An introduction to the pathophysiology of osteoarthritis. Front Biosci 1999;4:D662–70.
30. Poole AR, Rosenberg LC, Reiner A, Ionescu M, Bogoch E, Roughley PJ. Contents and distributions of the proteoglycans decorin and biglycan in normal and osteoarthritic human articular cartilage. J Orthop Res 1996;14:681–9.

31. Tesche F, Miosge N. Perlecan in late stages of osteoarthritis of the human knee joint. Osteoarthritis Cartilage 2004;12:852–62.
32. Chubinskaya S, Kuettner KE, Cole AA. Expression of matrix metalloproteinases in normal and damaged articular cartilage from human knee and ankle joints. Lab Invest 1999;79:1669–77.
33. Woessner Jr JF, Gunja-Smith Z. Role of metalloproteinases in human osteoarthritis. J Rheumatol Suppl 1991;27:99–101.
34. Hollander AP, Heathfield TF, Webber C, Iwata Y, Bourne R, Rorabeck C, *et al*. Increased damage to type II collagen in osteoarthritic articular cartilage detected by a new immunoassay. J Clin Invest 1994;93:1722–32.
35. Hollander AP, Heathfield TF, Webber C, Iwata Y, Bourne R, Rorabeck C, *et al*. Increased damage to type II collagen in osteoarthritic articular cartilage detected by a new immunoassay. J Clin Invest 1994;93:1722–32.
36. Stoop R, Buma P, van der Kraan PM, Hollander AP, Billinghurst RC, Meijers TH, *et al*. Type II collagen degradation in articular cartilage fibrillation after anterior cruciate ligament transection in rats. Osteoarthritis Cartilage 2001;9:308–15.
37. Hambach L, Neureiter D, Zeiler G, Kirchner T, Aigner T. Severe disturbance of the distribution and expression of type VI collagen chains in osteoarthritic articular cartilage. Arthritis Rheum 1998;41:986–96.
38. Radmacher M, Tillamnn RW, Fritz M, Gaub HE. From molecules to cells: imaging soft samples with the atomic force microscope. Science 1992;257:1900–5.
39. Roberts S, Ayad S, Menage PJ. Immunolocalisation of type VI collagen in the intervertebral disc. Ann Rheum Dis 1991;50:787–91.
40. Ahrens MJ, Dudley AT. Chemical pretreatment of growth plate cartilage increases immunofluorescence sensitivity. J Histochem Cytochem 2011;59:408–18.
41. Rolauffs B, Williams JM, Grodzinsky AJ, Kuettner KE, Cole AA. Distinct horizontal patterns in the spatial organization of superficial zone chondrocytes of human joints. J Struct Biol 2008;162:335–44.
42. Wilusz RE, Zauscher S, Guilak F. Micromechanical mapping of early osteoarthritic changes in the pericellular matrix of human articular cartilage. Osteoarthritis and cartilage/OARS. Osteoarthritis Res Soc 2013;21:1895–903, https://doi.org/10.1016/j.joca.2013.1008.1026.
43. Athanasiou KA, Rosenwasser MP, Buckwalter JA, Malinin TI, Mow VC. Interspecies comparisons of in situ intrinsic mechanical properties of distal femoral cartilage. J Orthop Res 1991;9:330–40.
44. Schinagl RM, Gurskis D, Chen AC, Sah RL. Depth-dependent confined compression modulus of full-thickness bovine articular cartilage. J Orthop Res 1997;15:499–506.
45. Coleman JL, Widmyer MR, Leddy HA, Utturkar GM, Spritzer CE, Moorman 3rd CT, *et al*. Diurnal variations in articular cartilage thickness and strain in the human knee. J Biomech 2013;46:541–7.
46. Darling EM, Wilusz RE, Bolognesi MP, Zauscher S, Guilak F. Spatial mapping of the biomechanical properties of the pericellular matrix of articular cartilage measured in situ via atomic force microscopy. Biophys J 2010;98:2848–56.
47. Wilusz RE, DeFrate LE, Guilak F. Immunofluorescence-guided atomic force microscopy to measure the micromechanical properties of the pericellular matrix of porcine articular cartilage. J R Soc Interface 2012;9:2997–3007.
48. Alexopoulos LG, Williams GM, Upton ML, Setton LA, Guilak F. Osteoarthritic changes in the biphasic mechanical properties of the chondrocyte pericellular matrix in articular cartilage. J Biomech 2005;38:509–17.
49. Horikawa O, Nakajima H, Kikuchi T, Ichimura S, Yamada H, Fujikawa K, *et al*. Distribution of type VI collagen in chondrocyte microenvironment: study of chondrons isolated from human normal and degenerative articular cartilage and cultured chondrocytes. J Orthop Sci 2004;9:29–36.
50. Melrose J, Roughley P, Knox S, Smith S, Lord M, Whitelock J. The structure, location, and function of perlecan, a prominent pericellular proteoglycan of fetal, postnatal, and mature hyaline cartilages. J Biol Chem 2006;281:36905–14.
51. Endothelial cells interact with the core protein of basement membrane perlecan through beta 1 and beta 3 integrins: an adhesion modulated by glycosaminoglycan. J Cell Biol 1992;119:945–59.
52. Brown JC, Sasaki T, Göhring W, Yamada Y, Timpl R. The C-terminal domain V of perlecan promotes pl integrin-mediated cell adhesion, binds heparin, nidogen and fibulin-2 and can be modified by glycosaminoglycans. Eur J Biochem 1997;250:39–46.
53. Gomes R, Kirn-Safran C, Farach-Carson MC, Carson DD. Perlecan: an important component of the cartilage pericellular matrix. J Musculoskelet Neuronal Interact 2002;2:511–6.
54. Prein C, Lagugne-Labarthet F, Beier F. Investigation of articular cartilage structural and biomechanical properties by atomic-force microscopy. Osteoarthritis Cartilage 2018;26:S400.
55. McLeod MA, Wilusz RE, Guilak F. Depth-Dependent anisotropy of the micromechanical properties of the extracellular and pericellular matrices of articular cartilage evaluated via atomic force microscopy. J Biomech 2013;46:586–92.
56. Cao L, Guilak F, Setton LA. Three-dimensional finite element modeling of pericellular matrix and cell mechanics in the nucleus pulposus of the intervertebral disk based on in situ morphology. Biomechanics Model Mechanobiol 2011;10:1–10.
57. Zelenski NA, Leddy HA, Sanchez-Adams J, Zhang J, Bonaldo P, Liedtke W, *et al*. Type VI collagen regulates pericellular matrix properties, chondrocyte swelling, and mechanotransduction in mouse articular cartilage. Arthritis Rheum 2015;67:1286–94.
58. Guilak F, Nims RJ, Dicks A, Wu CL, Meulenbelt I. Osteoarthritis as a disease of the cartilage pericellular matrix. Matrix Biol 2018;71–72:40–50.
59. Ronziere MC, Ricard-Blum S, Tiollier J, Hartmann DJ, Garrone R, Herbage D. Comparative analysis of collagens solubilized from human foetal, and normal and osteoarthritic adult articular cartilage, with emphasis on type VI collagen. Biochim Biophys Acta 1990;1038:222–30.
60. McDevitt CA, Pahl JA, Ayad S, Miller RR, Uratsuji M, Andrish JT. Experimental osteoarthritic articular cartilage is enriched in guanidine soluble type VI collagen. Biochem Biophys Res Commun 1988;157:250–5.
61. Xu X, Li Z, Leng Y, Neu CP, Calve S. Knockdown of the pericellular matrix molecule perlecan lowers in situ cell and matrix stiffness in developing cartilage. Dev Biol 2016;418:242–7.
62. Wilusz RE, DeFrate LE, Guilak F. A biomechanical role for perlecan in the pericellular matrix of articular cartilage. Matrix Biol 2012;31:320–7.
63. Soder S, Hambach L, Lissner R, Kirchner T, Aigner T. Ultrastructural localization of type VI collagen in normal adult and osteoarthritic human articular cartilage. Osteoarthritis Cartilage 2002;10:464–70.
64. Costa KD, Yin FC. Analysis of indentation: implications for measuring mechanical properties with atomic force microscopy. J Biomech Eng 1999;121:462–71.

65. Stolz M, Raiteri R, Daniels AU, VanLandingham MR, Baschong W, Aebi U. Dynamic elastic modulus of porcine articular cartilage determined at two different levels of tissue organization by indentation-type atomic force microscopy. Biophys J 2004;86:3269–83.

66. Park S, Costa KD, Ateshian GA, Hong KS. Mechanical properties of bovine articular cartilage under microscale indentation loading from atomic force microscopy. Proc Inst Mech Eng H 2009;223:339–47.